Volume 11 | Number 39 | 21 October 2015 | Pages 7699–7842

Soft Matter

www.softmatter.org

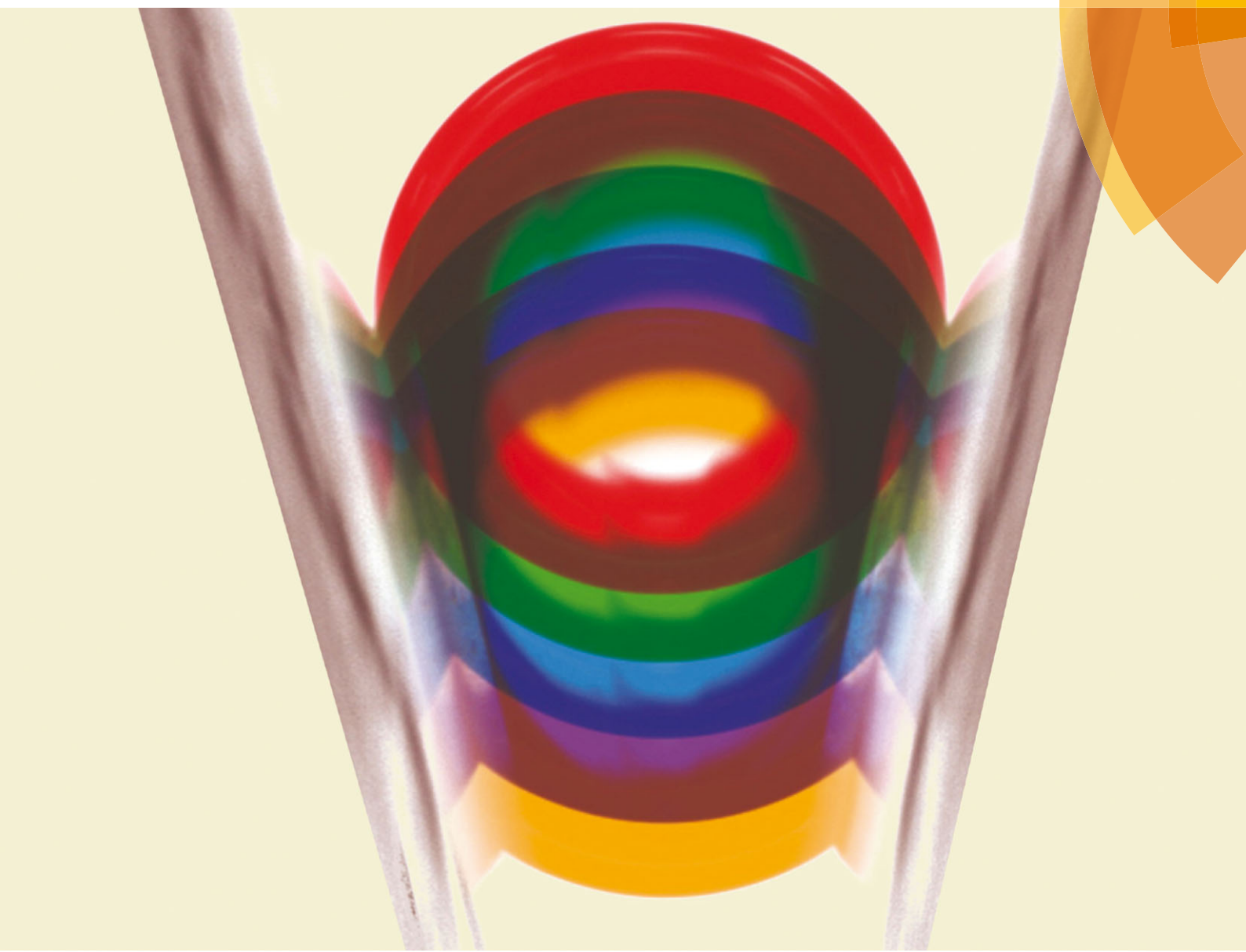

ISSN 1744-683X

ROYAL SOCIETY OF CHEMISTRY

PAPER
F. Mugele *et al.*
On the shape of a droplet in a wedge: new insight from electrowetting

Soft Matter

PAPER

View Article Online
View Journal | View Issue

Cite this: *Soft Matter*, 2015, 11, 7717

On the shape of a droplet in a wedge: new insight from electrowetting†

D. Baratian, A. Cavalli, D. van den Ende and F. Mugele*

Received 18th June 2015,
Accepted 13th July 2015

DOI: 10.1039/c5sm01511a

www.rsc.org/softmatter

The equilibrium morphology of liquid drops exposed to geometric constraints can be rather complex. Even for simple geometries, analytical solutions are scarce. Here, we investigate the equilibrium shape and position of liquid drops confined in the wedge between two solid surfaces at an angle α. Using electrowetting, we control the contact angle and thereby manipulate the shape and the equilibrium position of aqueous drops in ambient oil. In the absence of contact angle hysteresis and buoyancy, we find that the equilibrium shape is given by a truncated sphere, at a position that is determined by the drop volume and the contact angle. At this position, the net normal force between drop and the surfaces vanishes. The effect of buoyancy gives rise to substantial deviations from this equilibrium configuration which we discuss here as well. We eventually show how the geometric constraint and electrowetting can be used to position droplets inside a wedge in a controlled way, without mechanical actuation.

Introduction

Liquid bridges play an important role in our everyday life. On the beach we benefit from their stability when we build sand castles,[1] while in other situations liquid bridges can be annoying, for instance when they stick our hairs together after taking a shower.[2] These bridges exert attractive or repulsive forces on the contacting surfaces, which depend on the wettability of the substrates and affect the structural properties of a system. Studying the morphology of droplets and liquid bridges in complex geometries is thus relevant in many fields, such as droplet microfluidics,[3–5] fog harvesting and dropwise condensation,[6] and oil recovery.[7] Electrowetting provides us with a unique tool to control the wetting properties of a capillary system, and as such it has been applied extensively to analyze the interplay of wettability and complex geometries.[8,9] We have previously shown the electrowetting-induced displacement of a drop confined between a plain and a sphere, and described how the energy landscape of the drop is affected by hysteretic forces.[10] Electrowetting has also been employed to show wetting transitions for drops on fibers, which will take a ''clamshell'' or ''barrel'' configuration depending on the wettability of the fiber and the buoyancy of the system.[11]

Here, we consider a drop in a wedge, representing a minimal example of a complex geometry that is encountered very often, and as such has been studied extensively.[12–17] Surprisingly, in most of these studies only the dynamics of drop migration[17,18] or the motion of contact lines is investigated experimentally, which highly depend on the hysteretic properties of the surfaces involved.[14–16] However, studies of equilibrium liquid morphologies are mostly limited to analytical, mathematical or numerical approaches.[12,13] In this paper we use electrowetting to experimentally probe the equilibrium configurations for a droplet inside a wedge. We observe that the shape of the droplet is well described by a truncated sphere, which allows us to find a simple relation between the wettability of the wedge and the position of the drop. A force balance analysis shows that a truncated sphere droplet does not exert any force on the sidewalls of the wedge, an uncommon situation for constrained droplets. We also analyze the effect of buoyancy in the system, and the deformation of the droplet due to small, finite Bond numbers.

Methods and materials

The experimental setup is depicted in Fig. 1a and b. It consists of two substrates which are fixed at a certain angle α by means of a scaffold. The substrates are glass plates, on which transparent electrodes of indium tin oxide (ITO) are deposited. A layer of parylene-C is then added by a chemical vapor polymerization process, in order to form a dielectric layer on top of the electrode. The thickness of the insulating layer provides sufficient resistance against electrical breakdown in the electrowetting process. A parylene layer of 2 μm in thickness is suitable for our applied AC voltage in the range of 0–100 V RMS. To reduce the contact angle hysteresis on the substrates and to make the surface more hydrophobic, a thin layer of Teflon AF (DuPont, USA) is

Physics of Complex Fluids, MESA+ Institute for Nanotechnology, Department of Science & Technology, University of Twente, The Netherlands. E-mail: f.mugele@utwente.nl

† Electronic supplementary information (ESI) available. See DOI: 10.1039/c5sm01511a

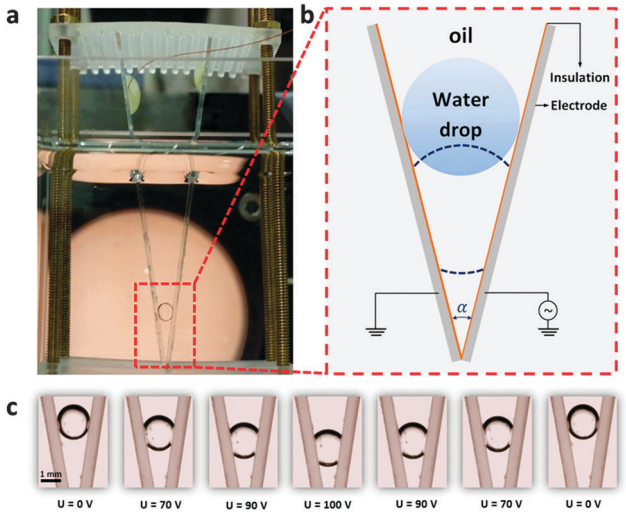

Fig. 1 (a) Experimental setup. The substrates are fixed at an angle using a scaffold, while immersed in a cuvette filled with oil. (b) Cross-sectional schematics of the drop configuration in a wedge with an opening angle of α. (c) Series of images of the drop, showing its position in the wedge at different voltages.

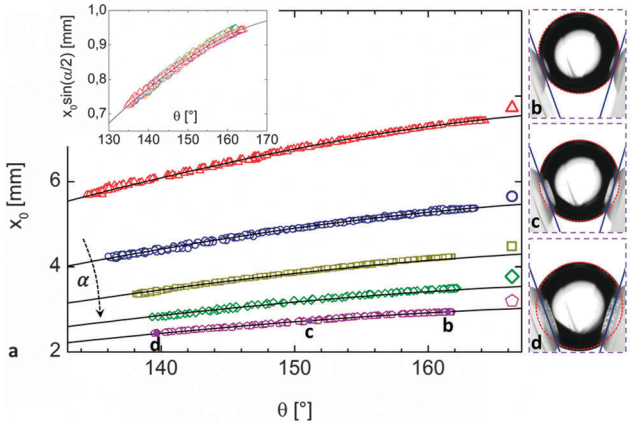

Fig. 2 (a) The distance of the center of the drop from the wedge apex x_0 is plotted as a function of the contact angle θ. Data is shown for a water droplet of 4 μL in volume, and for five wedges with opening angles of 15° (red triangles), 20° (blue circles), 26° (dark yellow squares), 32° (green diamonds), and 37° (purple pentagons). A comparison between our model predictions (solid black lines) and experimental results (scattered) is shown. Each data set is extracted from several voltage cycles (ramp up to 100 V and down to 0 V for at least 5 times). Inset: Collapsed data on the master curve. (b–d) Circular fit (red lines) of the side profile of drop at three different positions in the wedge ($\theta \simeq 140°, 151°, 162°$).

deposited through a dip-coating process along with a baking protocol. The surface shows a contact angle of $\theta_Y = 163°$ for our water/oil system. The contact angle hysteresis is as low as 1 degree (see ESI†).

The substrates are immersed into a quartz cuvette in order to perform the experiments in an oil environment. We use water droplets (conductivity of 5 mS cm^{-1} – KCl solution) inside bromohexadecane (Merck Millipore, USA) with a density of $\rho = 0.998$ g cm^{-3} for density matching experiments. Hexane ($\rho = 0.66$ g cm^{-3} Sigma-Aldrich, Germany) is used to test the effect of density mismatch on the shape of the drop. The voltage between the electrodes is applied at 1 kHz using a function generator (Agilent 33220A) together with a voltage amplifier (Trek PZD700A). The droplets in the wedge are imaged by uEye camera. We use an in-house image analysis MATLAB script to extract the profile of the droplets.

Experimental results

We start by considering a water droplet in bromohexadecane. The density matching of the two liquids results in a very small Bond number ($\simeq 10^{-3}$), and makes the effect of gravity negligible.

Fig. 1c shows selected snapshots from a typical experiment, in which a water drop of 4 μL in volume is released inside the wedge. Upon applying voltage between the electrodes, the contact angle decreases, and the droplet moves toward the apex of the wedge. When the voltage is decreased to zero, the drop moves back towards its initial position.

We observe that, for different values of the applied voltage, the profile of the droplet resembles a section of a circle, which implies that the overall shape of the droplet is a truncated sphere. This observation is corroborated by Fig. 2b–d, which show circular fits to the profile of the droplet, for contact angles of 140°, 151°, and 162°.

In Fig. 2a we plot the distance x_0 of the center of the droplet from the wedge apex as a function of the contact angle θ. For each recorded frame, the value of θ is obtained from the intersection of the wedge walls with the circular fits, while x_0 is the position of the center of the fitting circle. The data shown are collected over several cycles (at least 5), during which the voltage is slowly ramped up and down. We see that the displacement of the droplet is reliably reproduced over multiple cycles. We perform the experiment for a wide range of wedge angles α (see caption of Fig. 2), observing that for smaller α the droplet displacement is larger.

The almost perfect fits of Fig. 2b–d were achieved by eliminating all hysteretic and dynamic effects, *i.e.* by slowly approaching the desired voltage with loops of decreasing amplitude. If the voltage is monotonically changed, minor deformations in the shape of the moving droplet can be observed.

We also consider the effect of gravity, in the form of a small but finite Bond number ($\simeq 0.14$), on the shape of the droplet. To this end, we perform experiments in which the ambient liquid is replaced by hexane. The shape of the droplet in this case is depicted in Fig. 3d and e. It is clear that the droplet is now elongated, with a higher curvature at the bottom interface.

Geometric analysis and force balance

We will first consider the density matching scenario, in which the capillary length of the system $\lambda_c = (\sigma/g\Delta\rho)^{1/2}$ is much larger than the radius of the droplet $R \ll \lambda_c$: we therefore neglect the effect of gravity. If we assume a truncated spherical shape for the droplet, we can predict its radius and position inside the wedge.

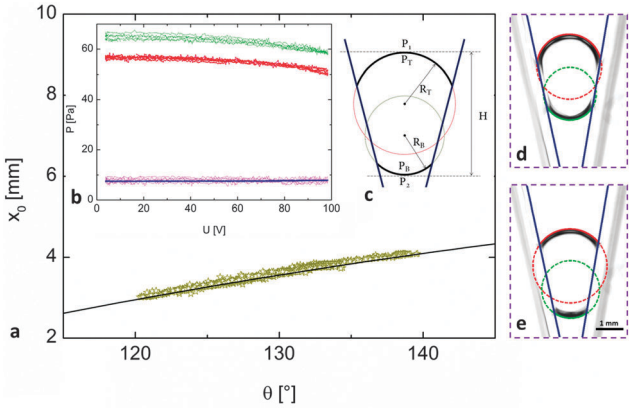

Fig. 3 (a) Droplet position in a wedge ($\alpha = 22^\circ$) for Bo $\simeq$ 0.14. The position of the center of the droplet is plotted *versus* the contact angle (dark yellow stars). (b) Pressure balance in the droplet. The difference between the Laplace pressure at the bottom interface (light green curve at the top) and the top interface (red curve in the middle) is shown in light purple (bottom scattering curve), and matches closely the hydrostatic pressure difference across the drop (bottom solid blue curve). (c) Sketch of the pressure balance in the droplet in case of density mismatch. (d) and (e) Fitting circles to the droplet profile for the top (red) and bottom (green) interfaces at 0 and 100 V, respectively.

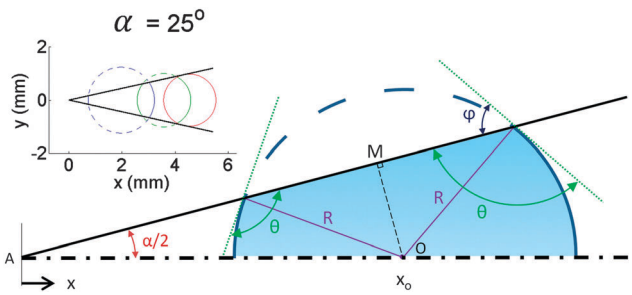

Fig. 4 Cross-sectional schematic of drop inside a wedge geometry. Only half of the symmetric system is shown. The drop, in the form of a truncated sphere of radius R, is located at a distance of x_0 from the wedge apex. Inset: Different morphologies of a drop of 4 μL volume inside a wedge of 25° opening angle $\theta_a = 180^\circ$ (red), $\theta_b = 140^\circ$ (green), and $\theta_c = 110^\circ$ (blue).

We assume that the walls are identical, smooth substrates without hysteresis. The droplet will then obtain the same contact angle θ_Y with each solid surface, as prescribed by Young's relation $\cos\theta_Y = (\sigma_{so} - \sigma_{sw})/\sigma$, where σ_{so}, σ_{sw}, and σ are the solid–oil, solid–water, and water–oil interfacial tensions, respectively.

Fig. 4 depicts a cross-sectional view of the droplet inside the wedge geometry. Here, α is the wedge opening angle, O is the center of the truncated sphere with radius R, and θ is the contact angle.

The volume V_{drop} of the droplet confined between the wedge walls can be calculated as: $\frac{1}{2}V_{drop} = V_{hs} - V_{cap}$, where $V_{hs} = \frac{2}{3}\pi R^3$ is the volume of a hemisphere and $V_{cap} = \frac{1}{3}\pi R^3(2 - 3\cos\varphi + \cos^3\varphi)$ the volume of the excluded spherical cap.

Since $\varphi + \theta = \pi$, so $\cos\varphi = -\cos\theta$, and we obtain $V_{drop} = \frac{2}{3}\pi R^3(\cos^3\theta - 3\cos\theta)$.

Because V_{drop} = constant, the radius R is a function of θ:

$$R(\theta) = \left(\frac{3V_{drop}}{2\pi\cos\theta(\cos^2\theta - 3)}\right)^{1/3} \quad (1)$$

We use x_0 to denote the distance between the wedge apex and the center of the truncated sphere. Since $\overline{OM} = R\cos\varphi = -R\cos\theta = x_0\sin(\alpha/2)$ we have:

$$x_0 = R(\theta)\frac{-\cos\theta}{\sin\alpha/2} = \left(\frac{3\cos^3\theta}{2\pi\cos\theta(3 - \cos^2\theta)}\right)^{1/3} \frac{V_{drop}^{1/3}}{\sin\alpha/2} \quad (2)$$

As a consequence of eqn (2), because the spherical morphology is only possible if the drop distance from the apex is larger than the radius of the droplet ($x_0/R \geq 1$), the condition $\frac{x_0}{R} = \frac{-\cos\theta}{\sin\alpha/2} \geq 1$ or $\theta \geq \theta_{min} = (\pi + \alpha)/2$ has to be satisfied. When the contact angle θ becomes smaller than θ_{min}, the liquid fills the corner and forms a spherical cap in the wedge. This is consistent with the conditions reported by Brinkmann *et al.*[13] for droplets in constrained geometries. They also discuss that a further reduction in the contact angle below $\theta_s = (\pi - \alpha)/2$ results in the liquid spreading along the wedge.[19] Distinct corner filling conditions have already been studied experimentally.[16,20] However, investigating these liquid morphologies is beyond the scope of this paper, as substrates are prone to damage by electrowetting due to the high electric field at their contact points.

In the following, we will consider the case $\theta \geq \theta_{min}$. Eqn (2) shows that the position of the drop inside the wedge is then uniquely defined by three parameters; the wedge angle α, the volume of the drop V_{drop}, and the contact angle θ.

The inset in Fig. 4 shows the profile and position of a drop of 4 μL inside a wedge with opening angle $\alpha = 25^\circ$ and the contact angle θ is set to 180°, 140°, and 110°. It can be seen that, for a smaller contact angle, the radius of the droplet increases, while the geometric center moves closer to the apex of the wedge.

The black curves In Fig. 2a represent the position predicted from eqn (2), for different values of α. We observe a very close agreement with the experimental data, further corroborating our truncated sphere hypothesis. Eqn (2) can also be rewritten as $x_0 V_{drop}^{-1/3}\sin\frac{\alpha}{2} = \left(3\cos^3\theta/2\pi\cos\theta(3 - \cos^2\theta)\right)^{1/3}$, and all the data collapse to a single curve when we plot $x_0 V_{drop}^{-1/3}\sin\frac{\alpha}{2}$ as a function of θ, as shown in the inset of Fig. 2a.

We can now address the question of whether the truncated sphere described by eqn (1) and (2) is an equilibrium morphology for the droplet. The answer consists of two separate parts: whether the shape of the droplet is in equilibrium, and whether the forces acting on its center of mass balance each other. Concerning the first point, we note that, as the curvature of the oil/water interface is constant for a sphere, the internal pressure of the droplet is homogeneous. This means that no flow takes place inside the droplet, and therefore no deformation can occur in its profile. The shape of the droplet is thus an equilibrium one.

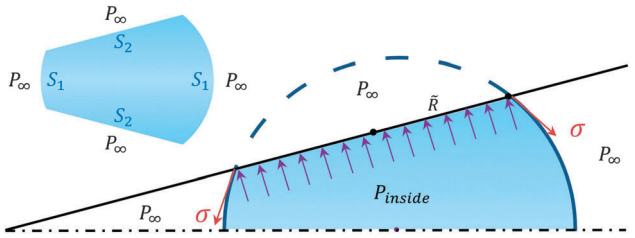

Fig. 5 Schematic of the forces exerted on the drop's contact area to the substrate. The red arrows show the surface tension contribution while the purple arrows represent the sum of forces associated with pressures inside and outside the droplet. Inset: The truncated spherical drop in an isopressure field when the substrate contribution is replaced with the equivalent values.

To evaluate the second point, we now consider the balance of the forces acting on the droplet.

As the cross section of a sphere and a plane is a circle, the droplet contact line on the substrate will be a circle of radius $\tilde{R}$; hence the contact area is $\pi\tilde{R}^2$ and the contour length is $2\pi\tilde{R}$.

The force on each single wedge substrate due to the presence of the drop is then given by:

$$\underline{F}_w = \left(2\pi\tilde{R}\sigma\sin\theta - \pi\tilde{R}^2(P_{inside} - P_\infty)\right)\underline{\hat{n}} \qquad (3)$$

where $\underline{\hat{n}}$ is the normal to the substrate pointing inwards the droplet, σ is the oil–water surface tension, P_{inside} is the pressure inside the droplet and P_∞ is the background pressure, as shown in Fig. 5.

At equilibrium, the shape of a liquid droplet is defined by the well-known Young–Laplace equation $P_{inside} - P_\infty = \Delta P = \sigma\kappa$ which relates the mean curvature of the free interface κ and the surface tension σ to the pressure difference ΔP across the oil–water interface. Since the drop has a truncated spherical shape with radius R, the curvature of the free surface is constant and given by: $\kappa = 2/R$. Thus $P_{inside} - P_\infty = 2\sigma/R$.

Considering the relation $\tilde{R} = R\sin\varphi = R\sin\theta$, and taking into account the force and pressure argument in eqn (3), we conclude that the force exerted on the wedge wall due to the presence of the droplet is equal to zero *i.e.* the force exerted by the droplet, $\pi\tilde{R}^2P_{inside} - 2\pi\tilde{R}\sigma\sin\theta$ is equal to the force due to the ambient liquid, $\pi\tilde{R}^2P_\infty$, acting on the backside of the substrate. This observation is quite interesting, especially in comparison to the widely encountered situation of sandwiched droplets between parallel plates. In that case, the droplet exerts an attractive or repulsive force on the plates. The only exception is when the distance between the plates and their wettability are such that the droplet assumes the shape of a truncated sphere. However, by tilting one of the plates, the droplet can maintain a spherical shape by moving sideways, so that for any contact angle larger than θ_{min} the droplet does not exert any force on the plates, regardless of the wedge opening and the volume of the drop.

As a consequence of eqn (3), the net force of each wedge substrate on the droplet is $\pi\tilde{R}^2P_\infty$. Hence the total force exerted on the droplet is given by:

$$\underline{F}_{drop} = \int_{S_1} -P_\infty\underline{e}_n\mathrm{d}S + \int_{S_2} -P_{inside}\underline{e}_n\mathrm{d}S + \int_{\partial S_2}\sigma\sin\theta\underline{e}_n\mathrm{d}l \qquad (4)$$

where $\underline{e}_n$ is a unit vector perpendicular to the drop interface, pointing outwards. At the contact area with the wedge walls, $\underline{e}_n = -\underline{\hat{n}}$. If we cut out the substrates and substitute the equivalent force exerted from the wedge walls to the drop, we find the droplet in an isopressure field (inset of Fig. 5) which results in a zero net force on the truncated spherical droplet.

$$\underline{F}_{drop} = -P_\infty\int_{S_1}\underline{e}_n\mathrm{d}S - P_\infty\int_{S_2}\underline{e}_n\mathrm{d}S = -P_\infty\int_S\underline{e}_n\mathrm{d}S = 0 \qquad (5)$$

Our geometric analysis thus shows that a truncated sphere is a viable geometry for the droplet, consistent with the geometric and volume constraint. Our force balance argument shows that no force acts on the center of mass of the droplet. We therefore conclude that the truncated sphere is an equilibrium configuration for the system.

This analysis shows that a spherical section is a solution of the Young–Laplace equation. However, there is no proof that such solution is unique.[21,22] Our experimental results are rather interesting in this light, as we directly observe the truncated sphere shape. Moreover, the position of the droplet matches closely the prediction of eqn (2). These observations show that, when contact angle hysteresis is negligible and the density of the droplet matches with the surrounding oil, the truncated sphere describes the equilibrium state of a droplet in a wedge very well.

Finally, we analyze the shape of the droplet when buoyancy is not negligible. Fig. 3d and e clearly show the different curvature of the top and bottom parts of the oil/water interface, with a higher Laplace pressure at the bottom to balance the hydrostatic component. This balance can be expressed as

$$\begin{aligned}\Delta\rho gH &= \sigma\kappa_{bottom} - \sigma\kappa_{top}\\ &= \sigma\left(\frac{1}{R_T} + \frac{1}{R_{out}^T}\right) - \sigma\left(\frac{1}{R_B} + \frac{1}{R_{out}^B}\right)\end{aligned} \qquad (6)$$

where H is the height of the droplet and R_T and R_B are top and bottom radii of curvature extracted from the profile of the droplet. R_{out}^T and R_{out}^B are the out-of-plane radii of curvature along the other symmetry plane of the droplet, calculated at the top and bottom interfaces of the droplet, respectively. We experimentally observe that the projection of the sphere on this plane can approximately be fitted by a single circle. This means that $R_{out}^T = R_{out}^B = R_{out}$, and the out-of-plane curvature does not significantly contribute to the pressure balance, which can be rewritten as: $\Delta\rho gH = \sigma\left(\frac{1}{R_T} - \frac{1}{R_B}\right)$. In Fig. 3b we plot the different pressure terms from eqn (6) extracted from our experiment. The purple line shows the difference between the Laplace pressure at the top (red) and bottom (green) of the droplet. We see that the this value matches closely the hydrostatic pressure contribution (in blue), meaning a complete pressure balance in the drop.

If we fit the whole interface with a single circular profile, we can again use eqn (2) to predict the expected position of the droplet. Fig. 3a shows the position x_0 of the center of the droplet as a function of the contact angle θ (yellow markers). Both quantities are calculated from the circular fit to the droplet profile, as in Fig. 2. The black line in Fig. 3a shows the model prediction.

While the fit of the shape of the droplet to a single sphere is not as good as in Fig. 2, we see that its position is still well captured. Therefore, such a small deviation from the truncated sphere shape do not significantly affect the position of the droplet in the wedge. This observation, combined with the pressure balance from eqn (6), provides a thorough description of the droplet even for small but finite Bond numbers.

Summary and conclusion

We used electrowetting to analyze the equilibrium shape and position of a droplet inside a wedge under different wettability conditions. Our experiments are in very good agreement with a simple analytic model, showing that the equilibrium shape of the droplet is a section of a sphere. While we cannot rule out the existence of other equilibrium configurations, we show that the spherical section model is descriptive and predictive over a wide range of contact angles and wedge openings. An interesting consequence is that we obtain a simple correlation between the position of the droplet inside the wedge and the contact angle of the system.

A finite buoyancy induces deformations in the equilibrium shape of the droplet, which we quantify. However, for small Bond numbers, the position of the droplet is still well captured by a truncated sphere description.

The precise and continuous control over the position of the droplet inside the wedge which we demonstrate suggests interesting applications in microfluidics. Compared to other designs that employ wedge geometries to move droplets, the ''electrowetting in a wedge'' approach is completely independent from mechanical actuation.[8] A natural application could arise from devices that already employ tapered micro-channel for other purposes, such as ''on-demand drop generation''.[4]

Acknowledgements

We thank R. de Ruiter and J. de Ruiter for their support in development of image analysis code and also for fruitful discussions. We acknowledge financial support by the Dutch Technology Foundation STW, which is part of the Netherlands Organization for Scientific Research (NWO), within the VICI program.

References

1 A. Kudrolli, Granular matter: sticky sand, *Nat. Mater.*, 2008, **7**(3), 174–175.
2 J. Bico, *et al.*, Adhesion: elastocapillary coalescence in wet hair, *Nature*, 2004, **432**(7018), 690.
3 S.-Y. Teh, *et al.*, Droplet microfluidics, *Lab Chip*, 2008, **8**(2), 198.
4 R. Dangla, S. C. Kayi and C. N. Baroud, Droplet microfluidics driven by gradients of confinement, *Proc. Natl. Acad. Sci. U. S. A.*, 2013, **110**(3), 853–858.
5 M. J. Jebrail, M. S. Bartsch and K. D. Patel, Digital microfluidics: a versatile tool for applications in chemistry, biology and medicine, *Lab Chip*, 2012, **12**(14), 2452.
6 C. Dorrer and J. Rühe, Condensation and Wetting Transitions on Microstructured Ultrahydrophobic Surfaces, *Langmuir*, 2007, **23**(7), 3820–3824.
7 C. Luo and X. Heng, Separation of Oil from a Water/Oil Mixed Drop Using Two Nonparallel Plates, *Langmuir*, 2014, **30**(33), 10002–10010.
8 A. Klingner, Electrowetting-induced morphological transitions of fluid microstructures, *J. Appl. Phys.*, 2004, **95**(5), 2918.
9 H. B. Eral, *et al.*, Drops on functional fibers: from barrels to clamshells and back, *Soft Matter*, 2011, **7**(11), 5138.
10 R. de Ruiter, *et al.*, Stability Limits of Capillary Bridges: How Contact Angle Hysteresis Affects Morphology Transitions of Liquid Microstructures, *Phys. Rev. Lett.*, 2015, **114**(23), 234501.
11 Y. Zheng, *et al.*, Directional water collection on wetted spider silk, *Nature*, 2010, **463**(7281), 640–643.
12 P. Concus and R. Finn, Discontinuous behavior of liquids between parallel and tilted plates, *Phys. Fluids*, 1998, **10**(1), 39.
13 M. Brinkmann and R. Blossey, Blobs, channels and ''cigars'': Morphologies of liquids at a step, *Eur. Phys. J. E: Soft Matter Biol. Phys.*, 2004, **14**(1), 79–89.
14 M. Prakash, D. Quere and J. W. M. Bush, Surface Tension Transport of Prey by Feeding Shorebirds: The Capillary Ratchet, *Science*, 2008, **320**(5878), 931–934.
15 J. W. M. Bush, *et al.*, On a tweezer for droplets, *Adv. Colloid Interface Sci.*, 2010, **161**(1–2), 10–14.
16 C. Luo, X. Heng and M. Xiang, Behavior of a Liquid Drop between Two Nonparallel Plates, *Langmuir*, 2014, **30**(28), 8373–8380.
17 J. Hong, *et al.*, Drop transport between two non-parallel plates *via* AC electrowetting-driven oscillation, *Sens. Actuators, B*, 2013, **188**, 637–643.
18 E. Reyssat, Drops and bubbles in wedges, *J. Fluid Mech.*, 2014, **748**, 641–662.
19 P. Concus and R. Finn, On the behavior of a capillary surface in a wedge, *Proc. Natl. Acad. Sci. U. S. A.*, 1969, **63**(2), 292–299.
20 C. Luo, M. Xiang and X. Heng, A Stable Intermediate Wetting State after a Water Drop Contacts the Bottom of a Microchannel or Is Placed on a Single Corner, *Langmuir*, 2012, **28**(25), 9554–9561.
21 J. McCuan, *Pac. J. Math.*, 1997, **180**, 291.
22 P. Concus, R. Finn and J. McCuan, *Indiana Univ. Math. J.*, 2001, **50**, 411.